Observation of Flux Reversal in a Symmetric Optical Thermal Ratchet

Sang-Hyuk Lee, Kosta Ladavac,* Marco Polin, and David G. Grier
Department of Physics and Center for Soft Matter Research, New York University, New York, New York 10003, USA
(Received 4 October 2004; published 22 March 2005)

We demonstrate that a cycle of three holographic optical trapping patterns can implement a thermal ratchet for diffusing colloidal spheres and that the ratchet-driven transport displays flux reversal as a function of the cycle frequency and the intertrap separation. Unlike previously described ratchet models, the approach we describe involves three equivalent states, each of which is locally and globally spatially symmetric, with spatiotemporal symmetry being broken by the sequence of states.

DOI: 10.1103/PhysRevLett.94.110601 PACS numbers: 05.60.Cd, 82.70.Dd, 87.80.Cc

Brownian motion cannot create a steady flux in a system at equilibrium. Nor can local asymmetries in a static potential energy landscape rectify Brownian motion to induce a drift. A landscape that varies in time, however, can eke a flux out of random fluctuations by breaking spatiotemporal symmetry [1–4]. Such flux-inducing time-dependent potentials are known as thermal ratchets [5,6], and their ability to bias diffusion has been proposed as a possible mechanism for transport by molecular motors and is being actively exploited for macromolecular sorting [7].

Most thermal ratchet models are based on spatially asymmetric potentials. Their time variation involves displacing or tilting them relative to the laboratory frame, modulating their amplitude, changing their periodicity, or some combination, usually in a two-state cycle. Chen demonstrated that a spatially symmetric potential still can induce drift in a cycle of three states, one of which allows for free diffusion [8]. This idea since has been refined [9] and generalized [10]. Thermal ratcheting in a spatially symmetric double-well potential was demonstrated for a colloidal sphere in a pair of intensity modulated optical tweezers [11]. Directed transport also has been induced in an atomic cloud by a symmetric rocking ratchet created with an optical lattice [12].

Creating space-filling potential energy landscapes required for most ratchet models is challenging. Furthermore, their relationship to the operation of natural thermal ratchets has proved difficult to establish. This Letter describes an experimental demonstration of a spatially symmetric thermal ratchet implemented with holographic optical traps [13–15]. The potential energy landscape in this system consists of a large number of discrete optical tweezers [16], each of which acts as a symmetric potential energy well for nanometer-to-micrometer-scale objects such as colloidal spheres. We arrange these wells so that colloidal spheres can diffuse freely in the interstitial spaces but are localized rapidly once they encounter a trap. A three-state thermal ratchet then requires only displaced copies of a single two-dimensional trapping pattern. Despite its simplicity, this ratchet model displays flux reversal [5,17] in which the direction of motion is controlled by the rate at which particles diffuse and the ratchet's cycling rate.

Often predicted, and inferred from the behavior of some natural molecular motors and semiconductor devices [5], flux reversal has been directly observed in comparatively few systems. Flux reversal arises as a consequence of stochastic resonance for a colloidal sphere hopping between the symmetric double-well potential of a dual optical trap [11]. Previous larger-scale demonstrations have focused on ratcheting of magnetic flux quanta through type-II superconductors in both the quantum mechanical [18] and classical [19] regimes or else have exploited the crossover from quantum mechanical to classical transport in a quantum dot array [20]. Unlike the present implementation, these exploit spatially asymmetric potentials and take the form of rocking ratchets [5]. A similar crossover-mediated reversal occurs for atomic clouds in symmetric optical lattices [12]. A hydrodynamic ratchet driven by oscillatory flows through asymmetric pores also shows flux reversal [21,22]. In this case, however, the force field is provided by the divergence-free flow of an incompressible fluid rather than a potential energy landscape, and so is an instance of a so-called drift ratchet [21]. Other pioneering implementations of classical force-free thermal ratchets also were based on asymmetric potentials but did not exhibit flux reversal [23–27].

Figure 1 shows the principle upon which the three-state optical thermal ratchet operates. The process starts out with a pattern of discrete optical traps, each of which can localize an object. The pattern in the initial state is schematically represented as three discrete potential energy wells, each of width σ and depth V_0, separated by distance L. A practical trapping pattern can include a great many optical traps organized into manifolds. The first pattern is extinguished after time T and replaced immediately with the second, which is displaced from the first by $L/3$. This is repeated in the third state with an additional step of $L/3$, and again when the cycle is completed.

If the traps in a given state overlap those in the state before, a trapped particle is transported deterministically forward. Repeating this cycle transfers the object in a

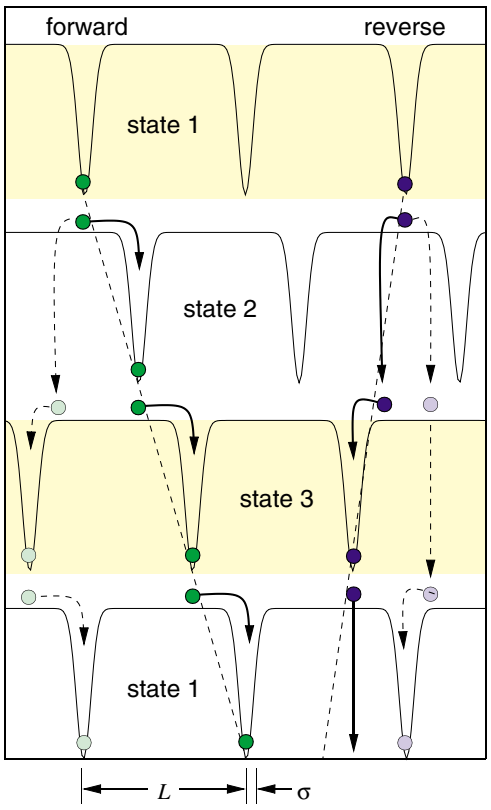

FIG. 1 (color online). A spatially symmetric three-state ratchet potential comprised of discrete potential wells.

direction determined by the sequence of states and is known as optical peristalsis [28]. The direction of motion can be reversed only by reversing the sequence.

The optical thermal ratchet differs from this in that the intertrap separation L is substantially larger than σ. Consequently, particles trapped in the first pattern are released into a force-free region and can diffuse freely when that pattern is replaced by the second. Those particles, such as the example labeled ''forward'' in Fig. 1, that diffuse far enough to reach the nearest traps in the second pattern rapidly become localized. A comparable proportion of this localized fraction then can be transferred forward in each successive step.

Unlike optical peristalsis, the stochastic ratchet transfers only a fraction of the particles in each cycle. This, however, leads to a new opportunity. Particles that miss the forward-going wave might still reach a trap on the opposite side of their starting point in the third state. These particles would be transferred *backward* by $L/3$ after time $2T$.

For particles of diffusivity D, the time required to diffuse the intertrap separation is $\tau = L^2/(2D)$. If we assume that particles begin each cycle well localized at a trap, and that the traps are well separated compared to their widths, then the probability for ratcheting forward by $L/3$ during the interval T is roughly $P_F \approx \exp[-(L/3)^2/(2DT)]$, while the probability of ratcheting backwards in time $2T$ is roughly $P_R \approx \exp[-(L/3)^2/(4DT)]$. The associated fluxes of particles then are $v_F = P_F L/(3T)$ and $v_R = -P_R L/(6T)$, with the dominant term determining the overall direction of motion. Flux reversal should occur when $T/\tau \lesssim (18\ln 2)^{-1} \approx 0.08$.

More formally, we can model an array of optical traps in the nth pattern as Gaussian potential wells,

$$V_n(x) = \sum_{j=-N}^{N} -V_0 \exp\left(-\frac{(x - jL - n\frac{L}{3})^2}{2\sigma^2}\right), \quad (1)$$

where $n = 0$, 1, or 2, and N sets the extent of the landscape. The probability density $\rho(x, t)dx$ for finding a Brownian particle within dx of position x at time t in state n evolves according to the master equation [29]

$$\rho(y, t + T) = \int P_n(y, T|x, 0)\rho(x, t)dx, \quad (2)$$

characterized by the propagator

$$P_n(y, T|x, 0) = e^{L_n(y)T}\delta(y - x), \quad (3)$$

where the Liouville operator for state n is

$$L_n(y) = D\left(\frac{\partial^2}{\partial y^2} + \beta\frac{\partial}{\partial y}V_n'(y)\right), \quad (4)$$

with $V_n'(y) = \frac{dV_n}{dy}$, and where β^{-1} is the thermal energy scale.

The master equation for a three-state cycle is

$$\rho(y, t + 3T) = \int P_{123}(y, 3T|x, 0)\rho(x, t)dx, \quad (5)$$

with the three-state propagator

$$P_{123}(y, 3T|x, 0) = \int dy_1 dy_2 P_3(y, T|y_2, 0)P_2(y_2, T|y_1, 0) \times P_1(y_1, T|x, 0). \quad (6)$$

Because the landscape is periodic and analytic, Eq. (5) has a steady-state solution such that

$$\rho(x, t + 3T) = \rho(x, t) \equiv \rho_{123}(x). \quad (7)$$

The mean velocity of this steady state then is given by

$$v = \int P_{123}(y, 3T|x, 0)\left(\frac{y - x}{3T}\right)\rho_{123}(x)dxdy, \quad (8)$$

where $P_{123}(y, 3T|x, 0)$ is the probability for a particle originally at position x to ''jump'' to position y by the end of one complete cycle, $(y - x)/(3T)$ is the velocity associated with making such a jump, and $\rho_{123}(x)$ is the fraction of the available particles actually at x at the beginning of the cycle in steady state. This formulation is invariant with respect to cyclic permutations of the states. The average velocity v therefore describes the time-averaged flux of particles.

Figure 2(a) shows numerical solutions of this system of equations for representative values of the relative interwell

separation L/σ. If the interval T between states is very short, particles are unable to keep up with the evolving potential energy landscape and so never travel far from their initial positions; the mean velocity vanishes in this limit. The transport speed v also vanishes as $1/T$ for large values of T because the induced drift becomes limited by the delay between states. If traps in consecutive patterns are close enough [$L = 6.5\sigma$ in Fig. 2(a)] particles jump forward at each transition with high probability, yielding a uniformly positive drift velocity. This transfer reaches its maximum efficiency for moderate cycle times, $T/\tau \approx 2\sqrt{2}(L/\sigma)(\beta V_0)^{-1}$. More widely separated traps [$L = 13\sigma$ in Fig. 2(a)] yield more interesting behavior. Here, particles are able to keep up with the forward-going wave for large values of T. Faster cycling, however, leads to flux reversal, characterized by negative values of v.

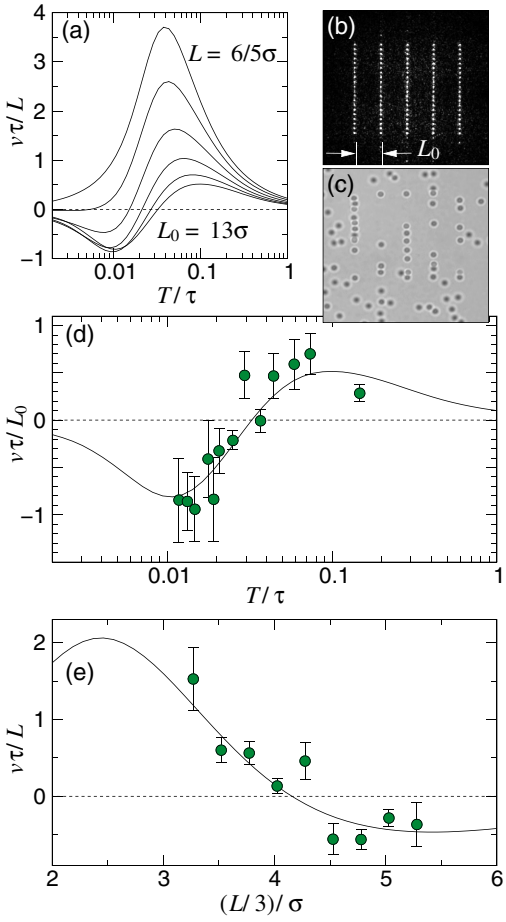

FIG. 2 (color online). (a) Crossover from deterministic optical peristalsis at $L = 6.5\sigma$ to thermal ratchet behavior with flux reversal at $L = 13\sigma$ for a three-state cycle of Gaussian well potentials at $\beta V_0 = 8.5$, $\sigma = 0.53$ μm, and $D = 0.33$ $\mu\mathrm{m}^2/\mathrm{sec}$. Intermediate curves are calculated for evenly spaced values of L. (b) Image of a 20×5 array of holographic optical traps at $L_0 = 6.7$ μm. (c) Image of colloidal silica spheres 1.53 μm in diameter interacting with the array. (d) Rate dependence of the induced drift velocity for fixed intertrap separation, L_0. (e) Separation dependence for fixed interstate delay, $T = 2$ sec.

We implemented this protocol for a sample of 1.53 μm diameter colloidal silica spheres (Bangs Laboratories, lot No. 5328) dispersed in water, using potential energy landscapes created from arrays of holographic optical traps [13–15]. The sample was enclosed in a sealed glass chamber 40 μm thick created by bonding the edges of a cover slip to a microscope slide and was allowed to equilibrate to room temperature ($21 \pm 1\,^{\circ}\mathrm{C}$) on the stage of a Zeiss S100TV Axiovert inverted optical microscope. A $100 \times$ NA (numerical aperture) 1.4 oil immersion SPlan Apo objective lens was used to focus the optical tweezer array into the sample and to image the spheres, whose motions were captured with an NEC TI 324A low noise monochrome CCD camera. The micrograph in Fig. 2(b) shows the focused light from a 20×5 array of optical traps formed by a phase hologram projected with a Hamamatsu X7550 spatial light modulator [30]. The tweezers are arranged in 20-trap manifolds 25 μm long separated by $L_0 = 6.7$ μm. Each trap is powered by an estimated 2.5 ± 0.4 mW of laser light at 532 nm. The particles, which appear in Fig. 2(c), are twice as dense as water and sediment to the lower glass surface, where they diffuse freely in the plane with a measured diffusion coefficient of $D = 0.33 \pm 0.03$ $\mu\mathrm{m}^2/\mathrm{sec}$, which reflects the influence of the nearby wall. Out-of-plane fluctuations were minimized by projecting the traps at the spheres' equilibrium height above the wall [31].

We projected three-state cycles of optical trapping patterns in which the manifolds in Fig. 2(b) were displaced horizontally by $-L_0/3$, 0, and $L_0/3$, with interstate delay times T ranging from 0.8 to 10 sec. The particles' motions were recorded as uncompressed digital video streams for analysis [32,33]. Between 40 and 60 particles were in the trapping pattern during a typical run, so that roughly 40 cycles sufficed to acquire reasonable statistics under each set of conditions without complications due to collisions. We also tracked particles outside the trapping pattern to monitor their diffusion coefficients and to ensure the absence of drifts in the supporting fluid. The results plotted in Fig. 2(d) reveal flux reversal at $T/\tau \approx 0.03$. Excellent agreement with Eq. (8) is obtained for $\beta V_0 = 8.5 \pm 0.8$ and $\sigma = 0.53 \pm 0.01$ μm.

The appearance of flux reversal as one parameter is varied implies that other parameters also should control the direction of motion [5]. Indeed, flux reversal is obtained in Fig. 2(e) as the intertrap separation is varied from $L = 5.1$ to 8.3 μm at fixed delay time, $T = 2$ sec. These results also agree well with predictions of Eq. (8), with no adjustable parameters. The same effect also should arise for different populations in a heterogeneous sample with different values of D, V_0, and σ [34,35]. In this case, distinct fractions can be induced to move simultaneously in opposite directions.

Such sensitivity of the transport direction to details of the dynamics also might play a role in the functioning of molecular motors such as myosin-VI whose retrograde motion on actin filaments compared with other myosins has excited much interest [36]. This molecular motor is known to be nonprocessive [37]; its motion involves a diffusive search of the actin filament's potential energy landscape, which nevertheless results in unidirectional hand-over-hand transport [38]. These characteristics are consistent with the present model's timing-based flux reversal mechanism and could provide a basis to explain how small structural differences among myosins could lead to oppositely directed transport.

Brian Koss contributed to the early stages of this project. We are grateful for Mark Ofitserov's many technical contributions. We also have benefited from conversations with Dean Astumian and Martin Bier, and more recently with Franco Nori and Stephen Quake. This work was supported by the National Science Foundation through Grants No. DBI-0233971 and No. DMR-0304906. S. L. acknowledges support from the Kessler Family Foundation.

*Dept. of Physics, James Franck Institute and Institute for Biophysical Dynamics, The University of Chicago, Chicago, IL 60637, USA.

[1] R. D. Astumian and M. Bier, Phys. Rev. Lett. **72**, 1766 (1994).
[2] J. Prost, J. F. Chauwin, L. Peliti, and A. Ajdari, Phys. Rev. Lett. **72**, 2652 (1994).
[3] J. F. Chauwin, A. Ajdari, and J. Prost, Europhys. Lett. **27**, 421 (1994).
[4] J. Rousselet, L. Salome, A. Ajdari, and J. Prost, Nature (London) **370**, 446 (1994).
[5] P. Reimann, Phys. Rep. **361**, 57 (2002).
[6] H. Linke, Appl. Phys. A **75**, 167 (2002).
[7] M. P. Hughes, Electrophoresis **23**, 2569 (2002).
[8] Y.-D. Chen, Phys. Rev. Lett. **79**, 3117 (1997).
[9] R. Kananda and K. Sasaki, J. Phys. Soc. Jpn. **68**, 3759 (1999).
[10] S. Savel'ev and F. Nori, Nat. Mater. **1**, 179 (2002).
[11] M. I. Dykman and B. Golding, in *Stochastic Processes in Physics, Chemistry and Biology*, edited by J. A. Freund and T. Pöschel (Springer-Verlag, Berlin, 2000), pp. 365–377.
[12] P. H. Jones, M. Goonasekera, and F. Renzoni, Phys. Rev. Lett. **93**, 073904 (2004).
[13] E. R. Dufresne and D. G. Grier, Rev. Sci. Instrum. **69**, 1974 (1998).
[14] E. R. Dufresne, G. C. Spalding, M. T. Dearing, S. A. Sheets, and D. G. Grier, Rev. Sci. Instrum. **72**, 1810 (2001).
[15] J. E. Curtis, B. A. Koss, and D. G. Grier, Opt. Commun. **207**, 169 (2002).
[16] A. Ashkin, J. M. Dziedzic, J. E. Bjorkholm, and S. Chu, Opt. Lett. **11**, 288 (1986).
[17] M. Bier and R. D. Astumian, Phys. Rev. Lett. **76**, 4277 (1996).
[18] G. Carapella, G. Costabile, N. Martucciello, M. Cirillo, R. Latempa, A. Polcari, and G. Filatrella, Physica (Amsterdam) **382C**, 337 (2002).
[19] J. E. Villegas, S. Savel'ev, F. Nori, E. M. Gonzalez, J. V. Anguita, R. Garcia, and J. L. Vicent, Science **302**, 1188 (2003).
[20] H. Linke, T. E. Humphrey, A. Löfgren, A. O. Sushkov, R. Newbury, R. P. Taylor, and P. Omling, Science **286**, 2314 (1999).
[21] C. Kettner, P. Reimann, P. Hänggi, and F. Müller, Phys. Rev. E **61**, 312 (2000).
[22] S. Matthias and F. Müller, Nature (London) **424**, 53 (2003).
[23] L. P. Faucheux, L. S. Bourdieu, P. D. Kaplan, and A. J. Libchaber, Phys. Rev. Lett. **74**, 1504 (1995).
[24] L. P. Faucheux, G. Stolovitzky, and A. Libchaber, Phys. Rev. E **51**, 5239 (1995).
[25] L. Gorre-Talini, J. P. Spatz, and P. Silberzan, Chaos **8**, 650 (1998).
[26] J. S. Bader, R. W. Hammond, S. A. Henck, M. W. Deem, G. A. McDermott, J. M. Bustillo, J. W. Simpson, G. T. Mulhern, and J. M. Rothberg, Proc. Nat. Acad. Sci. U.S.A. **96**, 13 165 (1999).
[27] J. S. Bader, M. W. Deem, R. W. Hammond, S. A. Henck, J. W. Simpson, and J. M. Rothberg, Appl. Phys. A **75**, 275 (2002).
[28] B. A. Koss and D. G. Grier, Appl. Phys. Lett. **82**, 3985 (2003).
[29] H. Risken, *The Fokker-Planck Equation* (Springer-Verlag, Berlin, 1989), 2nd ed.
[30] Y. Igasaki, F. Li, N. Yoshida, H. Toyoda, T. Inoue, N. Mukohzaka, Y. Kobayashi, and T. Hara, Opt. Rev. **6**, 339 (1999).
[31] S. H. Behrens, J. Plewa, and D. G. Grier, Euro. Phys. J. E **10**, 115 (2003).
[32] See EPAPS Document No. E-PRLTAO-94-084513 for a set of three MPEG-1 movies. A direct link to this document may be found in the online article's HTML reference section. The document may also be reached via the EPAPS homepage (http://www.aip.org/pubservs/epaps.html) or from ftp.aip.org in the directory /epaps/. See the EPAPS homepage for more information.
[33] J. C. Crocker and D. G. Grier, J. Colloid Interface Sci. **179**, 298 (1996).
[34] K. Ladavac, K. Kasza, and D. G. Grier, Phys. Rev. E **70**, 010901(R) (2004).
[35] M. Pelton, K. Ladavac, and D. G. Grier, Phys. Rev. E **70**, 031108 (2004).
[36] T. Hasson and R. E. Cheney, Curr. Opin. Cell Biol. **13**, 29 (2001).
[37] I. Lister, S. Schmitz, M. Walker, J. Trinick, F. Buss, C. Veigel, and J. Kendrick-Jones, EMBO J. **23**, 1729 (2004).
[38] Z. Okten, L. S. Churchman, R. S. Rock, and J. A. Spudich, Nature Struct. Mol. Biol. **11**, 884 (2003).